

Table 1: HHV of Ethanol, Butanol Isomers, and Gasoline

Compound	Ethanol [1]	Butanol Isomers [1]	Gasoline [2]
HHV [MJ/kg]	29.67	≈ 36	48.46

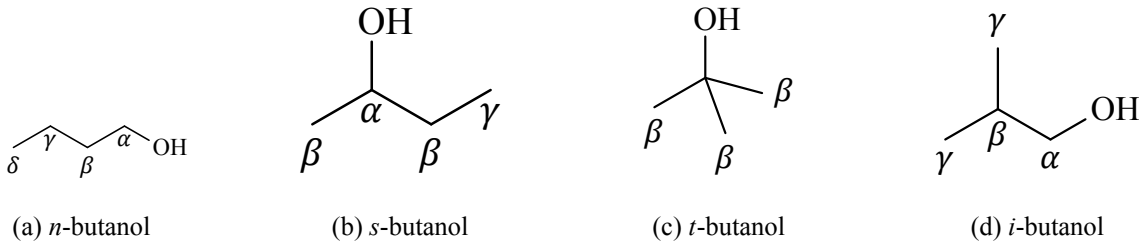


Figure 1: Skeletal structures of the butanol isomers

0.1 Structure of the Butanol Isomers

Butanol is the four carbon alcohol, and has four isomers: *n*-butanol (1-butanol); *s*-butanol (2-butanol); *t*-butanol (2-methyl-2-propanol); and *i*-butanol (2-methyl-1-propanol). The skeletal structures of the four isomers are shown in Fig. 1. The carbon atoms in the skeleton are labeled according to their distance from the hydroxyl moiety; the α carbon is the closest to the hydroxyl, followed by β , γ , and δ carbons. Not all of the butanols have all of the types of carbons listed here, due to varying chain lengths. For instance, *t*-butanol has one α carbon (not labeled), three β carbons, and no γ or δ carbons.

Three of the butanol isomers can be produced by biological pathways (*n*-, *s*-, and *i*-butanol) [3, 4], making them candidates for the “second-generation” of biofuels [3, 5]. Although *t*-butanol does not have an identified biological production pathway, it has commercial significance as an octane enhancer. In addition, the four isomers of butanol represent the smallest alcohol system with all four types of branching in the skeleton. This makes them excellent candidates to build kinetic models that can be extended to larger alcohols with similar structures.

Table 1 shows a comparison of the higher heating value of the butanol isomers with ethanol and gasoline. The higher energy density of the butanol isomers allows them to be blended in gasoline in

higher proportions and reduces the volumetric fuel economy (e.g. mpg) impact of replacing gasoline with biofuels.

0.2 Experimental Procedure

The reactants used in this study, along with their purities, are shown in Table 2. To determine the relative proportions of each reactant in the mixture, the absolute mass of fuel, the equivalence ratio (ϕ), and the oxidizer ratio ($X_{O_2} : X_{inert}$, where X indicates mole fraction) are specified. *s*- and *i*-Butanol are liquid at room temperature and have relatively low vapor pressure; therefore, each is massed in a syringe to within 0.01 g of the specified value. *t*-Butanol is solid at room temperature (melting point: 25 °C), and is melted before being handled in the same procedure as the other fuels. The 17 L mixing tank is vacuumed to an ultimate pressure less than 5 Torr prior to the injection of the liquid fuel through a septum. Proportions of O₂ and N₂ are added manometrically at room temperature. The preheat temperature of the RCM is set above the saturation point for each fuel to ensure complete vaporization. A magnetic stirrer mixes the reactants. The temperature inside the mixing tank is allowed to equilibrate for approximately 1.5 h.

This approach to mixture preparation has been validated in several previous studies by withdrawing gas samples from the mixing tank and analyzing the contents by GC/MS [6], GC-FID [7], and GC-TCD [8]. These studies have verified the concentration of *n*-butanol, *n*-decane, and water, respectively. In addition, both the work by Kumar et al. [7] on *n*-decane and the study of Weber et al. [6] on *n*-butanol confirmed that there was no fuel decomposition over the course of a typical set of experiments. Furthermore, within this study, each new mixture preparation is checked against previously tested conditions to ensure reproducibility.

Table 2 shows the experimental conditions considered in this study. The compressed pressure conditions have been chosen to match the previous *n*-butanol study [6], but also to provide data in regions not covered extensively in previous work. In addition, the fuel loading conditions have been chosen to complement previous work; the studies by Stranic et al. [9] and Moss et al. [10] used

Table 2: Experimental Conditions and Reactant Purities

Reactant (Purity)					Equivalence Ratio ϕ	Compressed Pressure P_C (bar)
<i>s</i> -butanol (99.99 %)	<i>i</i> -butanol (99.99 %)	<i>t</i> -butanol (99.99 %)	O ₂ (99.999 %)	N ₂ (99.995 %)		
Mole Percentage						
3.38			20.30	76.32	1.0	15
3.38			20.30	76.32	1.0	30
	3.38		20.30	76.32	1.0	15
	3.38		20.30	76.32	1.0	30
		3.38	20.30	76.32	1.0	15
		3.38	20.30	76.32	1.0	30
		1.72	20.65	77.63	0.5	30
		6.54	19.63	73.83	2.0	30
	1.72		20.65	77.63	0.5	15
	1.72		20.65	77.63	0.5	30
	3.38		40.60	56.02	0.5	15
	3.38		40.60	56.02	0.5	30
	3.38		10.15	86.47	2.0	30
	3.38		10.15	86.47	2.0	30

relatively dilute mixtures, so we have included higher fuel loading conditions. Furthermore, the compressed temperature conditions we have studied ($T_C = 715\text{ K}$ to 910 K) have not been examined in any other study, to our knowledge.

0.3 Experimental Results

0.3.1 Comparison of Butanol Isomers Ignition

Figure 2 shows the ignition delays of the four isomers of butanol measured in the RCM, at compressed pressure of $P_C = 15\text{ bar}$ for stoichiometric mixture in air. The dashed line for each isomer is a least squares fit to the data. The vertical error bars are two standard deviations of the measurements of the ignition delay. The standard deviation is computed based on all the runs at a particular compressed temperature and pressure condition, as discussed in ?? . The uncertainty in T_C was estimated in ??

to be approximately 2 % to 3 %.

Figure 2 demonstrates the differences in reactivity between the isomers for stoichiometric fuel/air mixtures at compressed pressure $P_C = 15$ bar. *n*-Butanol is clearly the most reactive, followed by *s*- and *i*-butanol, which have very similar reactivities in this temperature and pressure range. *t*-Butanol is the least reactive.

The order of reactivity found in the RCM at 15 bar agrees with the ST study at higher temperatures (approximately 1275 K to 1667 K) and lower pressure (1.5 atm) by Stranic et al. [9] but differs slightly from the studies of Moss et al. [10] who measured ignition delays in a ST near 1.5 atm and between 1275 K to 1400 K, and Veloo and Egolfopoulos [11] who measured atmospheric-pressure laminar flame speeds. In particular, Moss et al. [10] and Veloo and Egolfopoulos [11] found distinct differences in reactivity between *s*- and *i*-butanol, but the present study and the study by Stranic et al. [9] found that they were nearly indistinguishable in terms of reactivity under the conditions investigated. In addition, Stranic et al. [9] noted some disagreement between their ST ignition data and the data of Moss et al. [10] but their attempts to isolate the cause could not discern what the difference might be caused by.

Further, the order of the reactivity of the butanol isomers shows complex temperature and pressure dependence. This is demonstrated by the results shown in Fig. 3. In Fig. 3, the order of reactivity is different than in Fig. 2, where the only variation between the plots is the compressed pressure; in Fig. 3 the compressed pressure is $P_C = 30$ bar. Fig. 3 shows *i*-butanol to be the least reactive, *s*-butanol to be less reactive than but similar to *t*-butanol, and *n*-butanol to be the most reactive. Interestingly, the results of the ST study by Stranic et al. [9] differ from those in the current study at higher pressure, despite the agreement at lower pressure. In their study, Stranic et al. [9] found *i*- and *n*-butanol to have similar reactivity near 43 atm in the temperature range of 1020 K to 1280 K, whereas in the present study we find *i*-butanol to be the least reactive of all four isomers at a pressure of 30 bar and over the temperature range (715 K to 910 K) investigated.

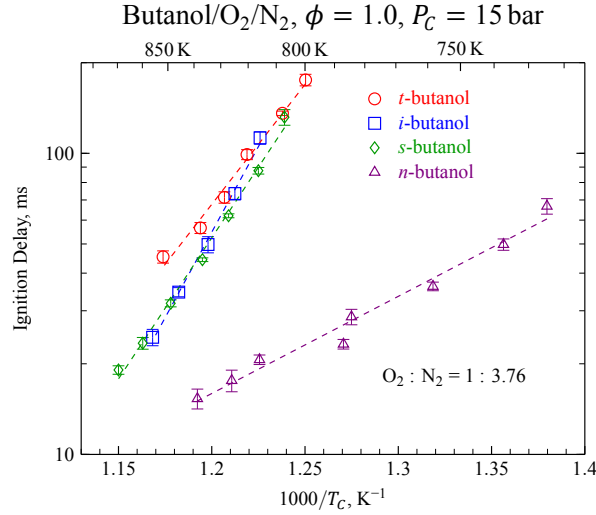


Figure 2: Ignition delays of the four isomers of butanol at compressed pressure $P_C = 15$ bar. Dashed lines are least squares fits to the data.

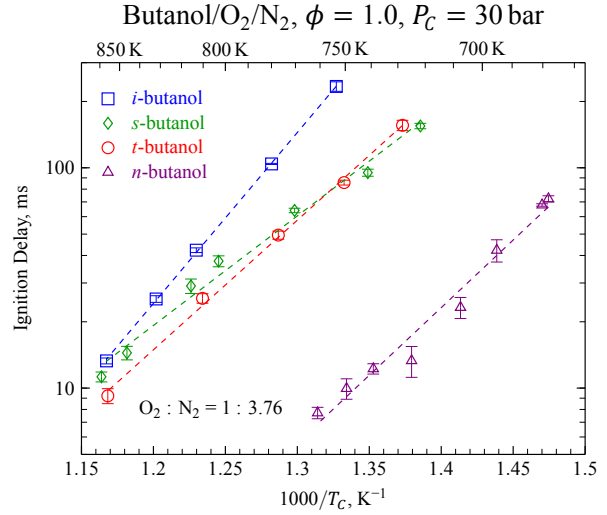


Figure 3: Ignition delays of the four isomers of butanol at compressed pressure $P_C = 30$ bar. Dashed lines are least squares fits to the data.

0.3.2 Ignition of *t*-Butanol

The fact that *t*-butanol becomes relatively more reactive than *i*- and *s*-butanol as pressure increases is surprising at first glance, and the reasons are not immediately apparent. Closer examination of the pressure traces for each experiment gives one clue as to the cause of the increased reactivity. Figure 4 shows the pressure traces for the *t*-butanol experiments at 15 bar for stoichiometric mixtures in air. It is evident that there is some pre-ignition heat release, because the reactive pressure trace diverges from the non-reactive case prior to the ignition event. Of the other isomers of butanol, only *n*-butanol shows any visible heat release prior to the main ignition event at 15 bar.

Figure 5 shows the pressure traces for *t*-butanol experiments at 30 bar for stoichiometric mixtures in air. The effect of pre-ignition heat release is even more striking in this figure, with substantial changes in the slope of the pressure trace during the reactive runs. Comparison to the pressure traces of the other isomers once again shows that the magnitude of the pre-ignition heat release for *t*-butanol is much greater. Despite the appearance of early pressure rise, which is typically indicative of two-stage ignition and low temperature chain branching, we do not find a negative temperature coefficient region in terms of the ignition delay response for any *t*-butanol experiments. Therefore,

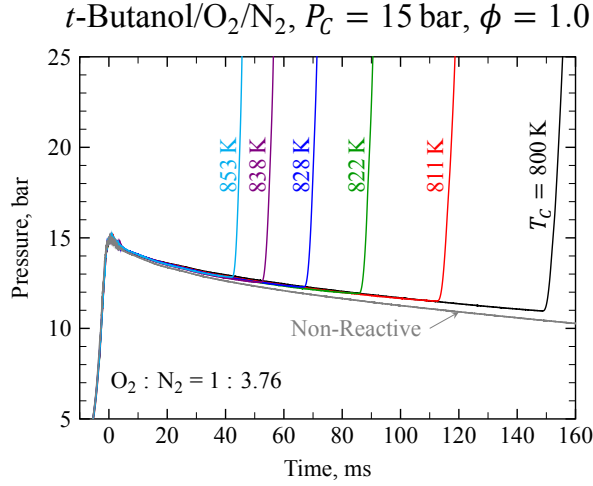


Figure 4: Pressure traces of the 15 bar *t*-butanol experiments, in stoichiometric air.

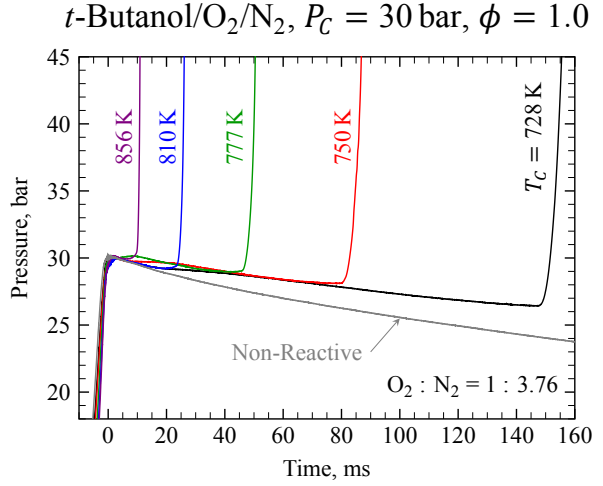


Figure 5: Pressure traces of the 30 bar *t*-butanol experiments, in stoichiometric air.

we adopt the phrase “pre-ignition heat release” rather than “two-stage ignition” in this work.

In an effort to understand the reactions causing the pre-ignition heat release, further experiments are conducted for *t*-butanol at $P_C = 30$ bar, for equivalence ratios of 0.5 and 2.0 in air. Figure 6 shows Arrhenius plots of the ignition delays for the three equivalence ratios. As with the previous *n*-butanol experiments at 15 bar [6] $\phi = 0.5$ is the least reactive and $\phi = 2.0$ is the most reactive. The slopes are similar, indicating that the overall activation energies are similar for the conditions investigated.

A more interesting comparison is of the pressure traces of the three equivalence ratios. It is clear from Figs. 5, 7, and 8 that there are qualitative differences in the pre-ignition heat release between the three equivalence ratios. This is most likely due to the effect of the increased (reduced) fuel mole fraction in the $\phi = 2.0$ ($\phi = 0.5$) case, since the mole fraction of fuel is changed by +93 % (-49 %) compared to the $\phi = 1.0$ case, while the mole fraction of oxygen changes by only -3 % (+2 %) compared to the $\phi = 1.0$ case, as shown in Table 2. Therefore, it appears that the qualitative change in pre-ignition behavior is due to the change of fuel mole fraction, where higher fuel loading promotes pre-ignition heat release.

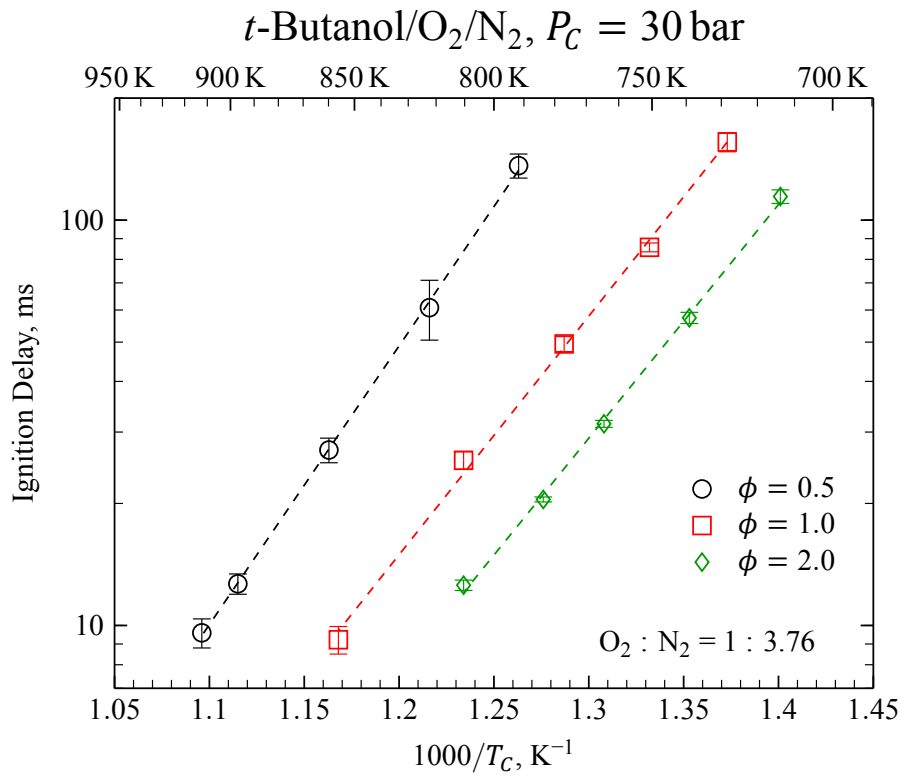


Figure 6: Ignition delays of three equivalence ratios of *t*-butanol in air, for $P_C = 30$ bar. Lines represent least squares fits to the data.

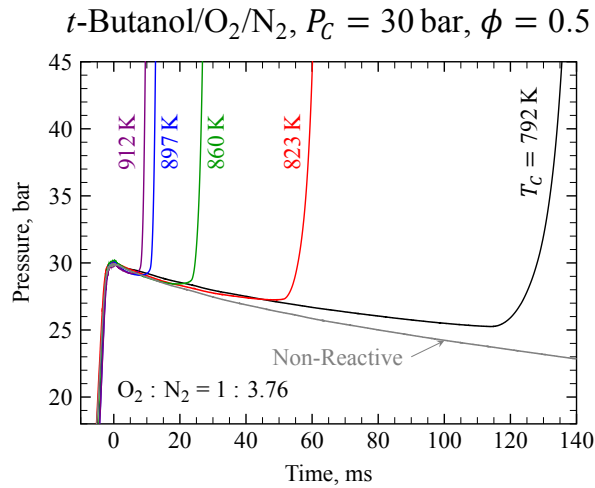


Figure 7: Pressure traces of the 30 bar *t*-butanol experiments, $\phi = 0.5$ in air.

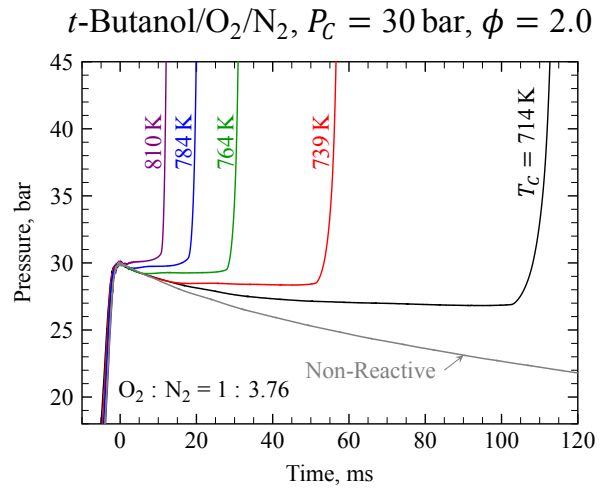


Figure 8: Pressure traces of the 30 bar *t*-butanol experiments, $\phi = 2.0$ in air.

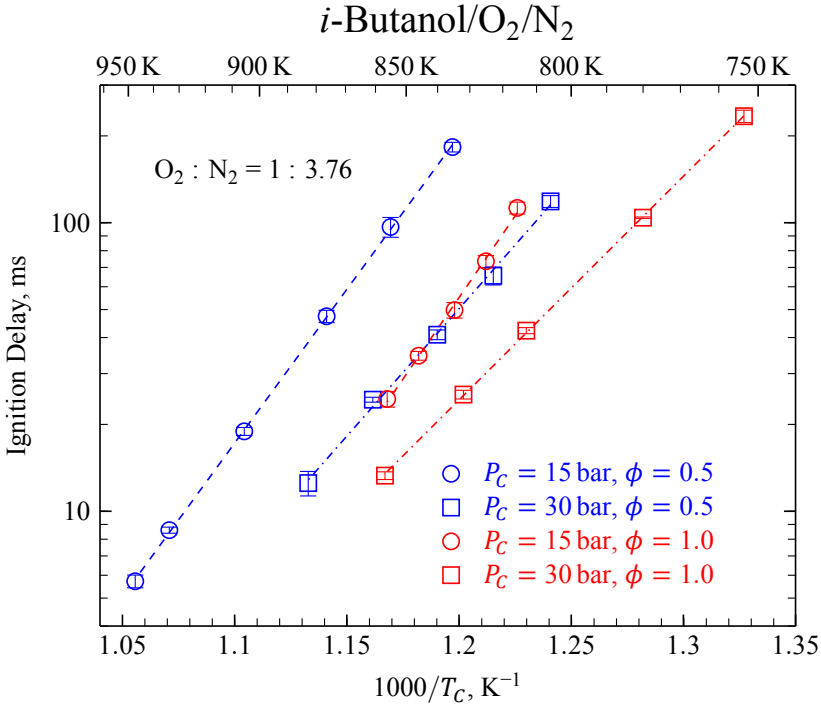


Figure 9: Comparison of the experimentally measured ignition delays of *i*-butanol at two compressed pressures, $P_C = 15$ bar (circles) and $P_C = 30$ bar (squares), and two equivalence ratios, $\phi = 0.5$ (blue) and $\phi = 1.0$ (red).

0.3.3 Ignition of *i*-Butanol

The experimental ignition delays of *i*-butanol measured at $P_C = 15$ bar and 30 bar and $\phi = 0.5$ in oxygen/nitrogen air are shown in Fig. 9. The error bars are equal to twice the standard deviation of all the runs at that condition. The lines are curve fits to the data. The circles represent the 15 bar data, while the squares represent the 30 bar data. Also shown in Fig. 9 are the experimental ignition delays presented in Sec. 0.3.1 at $\phi = 1.0$ and $P_C = 15$ bar and 30 bar. The $\phi = 0.5$ cases are shown in blue and the $\phi = 1.0$ cases are shown in red.

For both equivalence ratios, the 15 bar cases are less reactive than the 30 bar cases, as judged by the inverse of the ignition delay. Furthermore, in comparing the $\phi = 1.0$ data to the $\phi = 0.5$ data at the same compressed pressure, it is seen that the strong equivalence ratio dependence of the ignition delays previously measured for two other isomers of butanol, *n*-butanol [6] and *t*-butanol (Sec. 0.3.2), is also present for *i*-butanol.

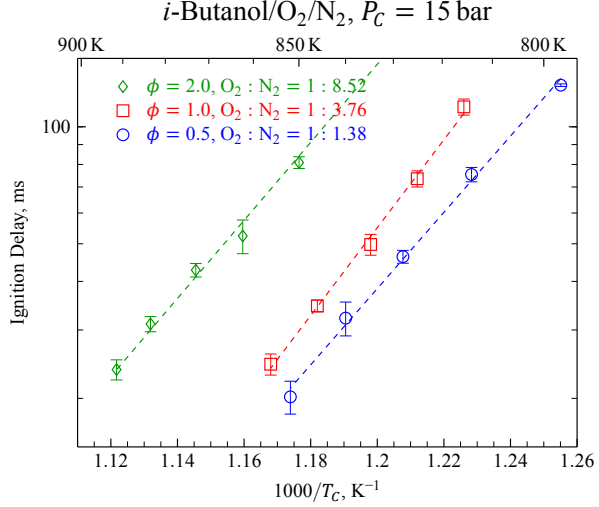


Figure 10: Comparison of the experimentally measured ignition delays of *i*-butanol at three equivalence ratios and $P_C = 15$ bar. The equivalence ratio is changed by varying the initial oxygen mole fraction at constant initial fuel mole fraction.

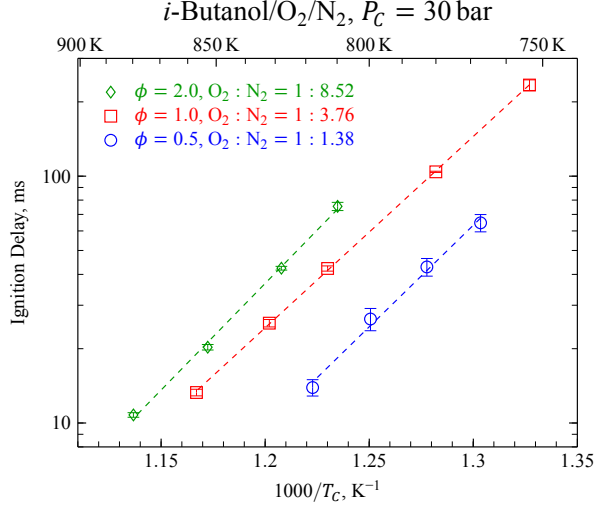


Figure 11: Comparison of the experimentally measured ignition delays of *i*-butanol at three equivalence ratios and $P_C = 30$ bar. The equivalence ratio is changed by varying the initial oxygen mole fraction at constant initial fuel mole fraction.

Figures 10 and 11 show the ignition delays of *i*-butanol at three equivalence ratios $\phi = 0.5, 1.0$, and 2.0 and $P_C = 15$ bar and 30 bar respectively. In these figures, the equivalence ratio is varied by holding the initial fuel mole fraction constant and varying the oxygen and nitrogen mole fractions. The ignition delay of *i*-butanol depends strongly on the initial oxygen mole fraction, similar to the trend shown for *n*-butanol [6].

0.4 Simulation Results

0.4.1 Comparison of Simulated Butanol Isomers Ignition

Simulations are performed with the kinetic mechanism from Sarathy et al. [12] denoted as the Sarathy et al. mechanism. Other recent mechanisms, such as the mechanism from Frassoldati et al. [13] do not include low temperature chemistry and are therefore unable to reproduce the low-temperature ignition delays measured in this study. The study by Sarathy et al. [12] validated their model for a wide set of the existing experimental data. In terms of ignition delays, this included the data from

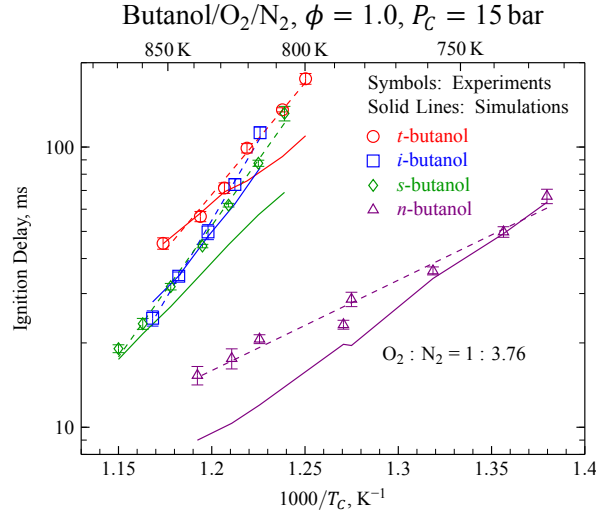


Figure 12: $P_C = 15$ bar, stoichiometric mixtures in air. Comparison of VPRO simulations using the kinetic mechanism of Sarathy et al. [12] with experimental ignition delays.

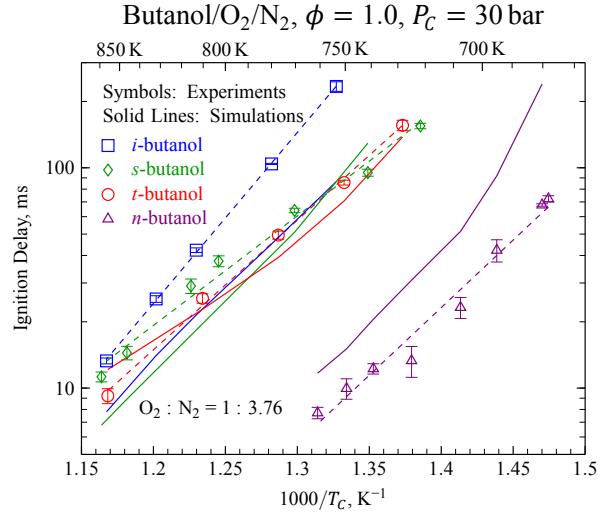


Figure 13: $P_C = 30$ bar, stoichiometric mixtures in air. Comparison of VPRO simulations using the kinetic mechanism of Sarathy et al. [12] with experimental ignition delays.

the study of Stranic et al. [9] up to 48 atm, our previous study on *n*-butanol [6], and the data being published in this study at 15 bar. Importantly, the mechanism of Sarathy et al. [12] was validated only for the 15 bar RCM data for all four isomers, but not the 30 bar data also being published here. The MIT mechanism [14, 15] was validated for *i*-butanol experiments, including pyrolysis and low pressure premixed flames; although the model includes all four isomers of butanol as reactants, it has not been optimized for any of the isomers except *i*-butanol.

Figures 12 and 13 show comparison of the VPRO simulations with the experimental data using the mechanism of Sarathy et al. [12]. As Sarathy et al. [12] showed in their work (and as we show here in Fig. 12), they found good agreement of the model predictions with the present RCM data at 15 bar. At $P_C = 30$ bar (Fig. 13), similar degree of agreement is found for *t*-butanol and *s*-butanol compared to $P_C = 15$ bar, although the *s*-butanol results are under-predicted at high temperature and over-predicted at low temperature. While the model of Sarathy et al. [12] is able to well capture the overall activation energy of *i*-butanol, it under-predicts the experimental data by about a factor of 2 to 3. The *n*-butanol data are over-predicted by a factor of about 1.5. Nevertheless, this agreement is quite good, especially considering that the model is not validated for these conditions.

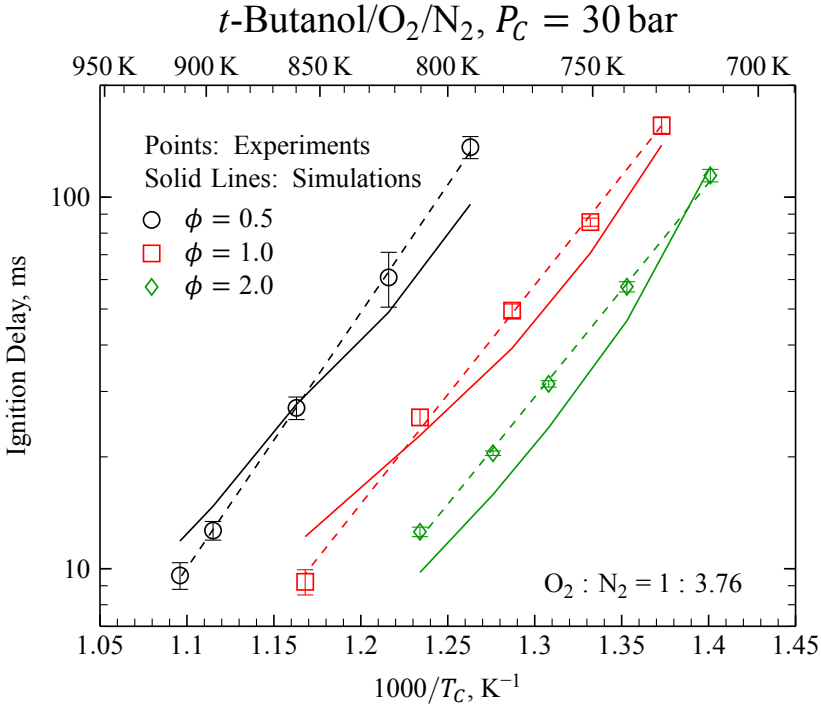


Figure 14: Comparison of the simulations using the kinetic mechanism of Sarathy et al. [12] for three equivalence ratio mixtures of *t*-butanol in air at $P_C = 30$ bar.

0.4.2 Simulated *t*-Butanol Ignition

The agreement of the mechanism by Sarathy et al. [12] with the off-stoichiometric mixtures of *t*-butanol is also quite good, as shown in Fig. 14. Figures 15a, 15b, and 15c show more detailed comparisons of the simulated pressure traces and the experimental results, for similar temperatures at the three equivalence ratios, respectively. Clearly, the simulations also exhibit some pre-ignition heat release. In general, the simulations qualitatively predict the pre-ignition heat release behavior at all three equivalence ratios. The $\phi = 0.5$ case has the least heat release and the $\phi = 2.0$ case has the most. Although the simulations are unable to match the heat release behavior quantitatively, they match the experimental ignition delays quite well. Considering the model is not validated for this temperature, pressure, and equivalence ratio regime, the mismatch of the pre-ignition behavior may not be of critical importance, depending on the application.

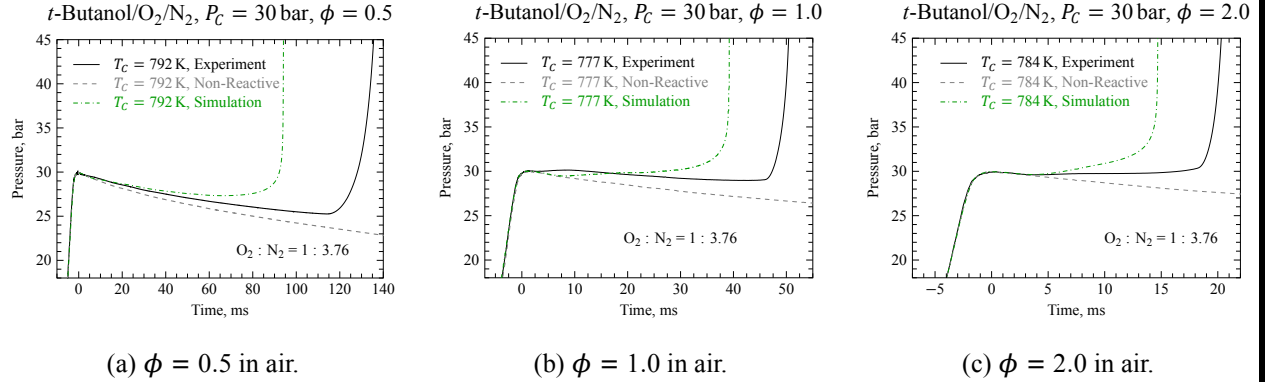


Figure 15: Pressure traces of selected *t*-butanol experiments compared with the corresponding non-reactive and simulated traces, using the mechanism of Sarathy et al. [12].

0.4.3 Simulated *i*-Butanol Ignition

In addition to the model by Sarathy et al. [12] which is validated for all four isomers of butanol, a kinetic model for the combustion of *i*-butanol has been developed and presented by Hansen et al. [14] and Merchant et al. [15]. This model has been validated for species profiles measured in a low-pressure, premixed flame by Hansen et al. [14], an atmospheric pressure diffusion flame by Grana et al. [16], and a doped methane flame by McEnally and Pfefferle [17], ignition delays measured by Stranic et al. [9], JSR species profiles measured by Togbé et al. [18], laminar flame speeds measured by Veloo and Egolfopoulos [11] and Liu et al. [19], and species profiles from a pyrolysis reactor Merchant et al. [15].

Recently, the *i*-butanol model developed by Hansen et al. [14] and Merchant et al. [15] has been updated with new reaction rates and pathways. The updates are detailed in the work of Weber et al. [20]. The primary updates were to add detailed low-temperature peroxy pathways involving *i*-butanol and its primary radicals. This model is still undergoing validation, but is presented here as the state-of-the-art in butanol modeling. This kinetic model will be referred to as the MIT mechanism.

In Fig. 16, VPRO simulations at 15 bar and 30 bar using the Sarathy et al. mechanism [12] and the MIT mechanism [20] are shown for *i*-butanol. Some conditions using the MIT mechanism did not ignite during the simulated time (approximately 800 ms), so those points are not shown in

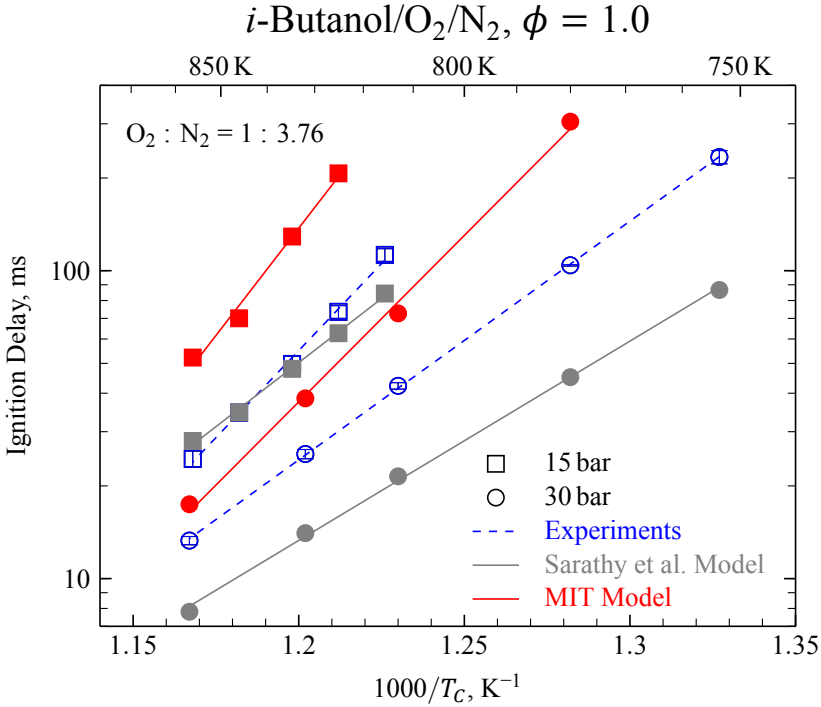


Figure 16: Comparison of VPRO simulations using the kinetic mechanism of Sarathy et al. [12] (gray) and the MIT mechanism [14, 15] (red) with the experimental ignition delay results (blue) for stoichiometric mixtures of *i*-butanol in air at $P_C = 15$ bar (squares) and $P_C = 30$ bar (circles).

Fig. 16. The mechanism by Sarathy et al. is in better agreement with the experiments at 15 bar than the MIT model. At 30 bar the MIT model over-predicts the ignition delay—as at 15 bar—while the Sarathy et al. mechanism under-predicts the ignition delay.

Figures 17 and 18 show comparisons of VPRO simulations using the MIT mechanism with the experimental data at three equivalence ratios with constant initial fuel mole fraction. In general, the model is unable to predict the oxygen concentration dependence of the ignition delays. A similar result was found for the comparison of *n*-butanol experiments with a model constructed using the same principles as the present model for *i*-butanol [6]. Moreover, comparing the experimental results with modeling results using the mechanism of Sarathy et al. [12] reveals a similar qualitative discrepancy, although the Sarathy et al. model tends to under-predict the experimental ignition delays whereas the MIT model tends to over-predict the experimental values. The reason for these diverging predictions will be explored and discussed in Sec. 0.5.1.

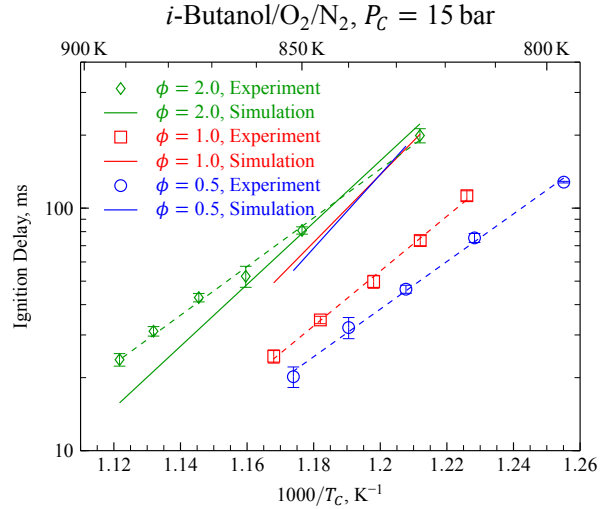


Figure 17: Comparison of the experimentally measured ignition delays of *i*-butanol at three equivalence ratios and $P_C = 15$ bar with VPRO simulations using the MIT mechanism.

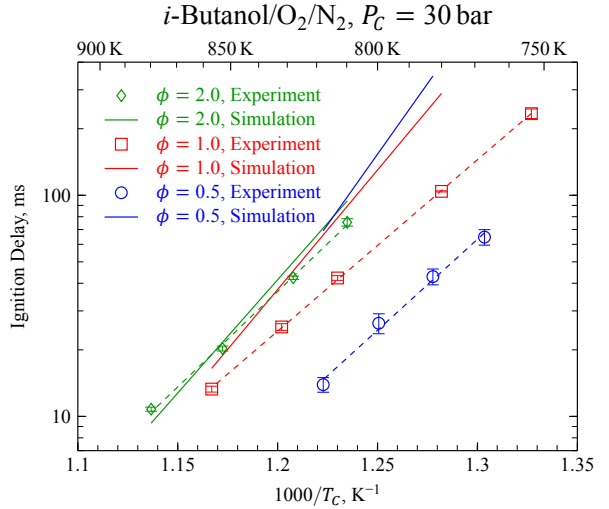


Figure 18: Comparison of the experimentally measured ignition delays of *i*-butanol at three equivalence ratios and $P_C = 30$ bar with VPRO simulations using the MIT mechanism.

0.5 Discussion

The relatively good agreement of the mechanism of Sarathy et al. [12] with the experimental data as shown in Figs. 12 and 13, even for conditions at which the mechanism has not been validated, suggests that using the mechanism to further interpret the experimental data is a worthwhile exercise. In particular, Figs. 19–22 show the initial steps of the fuel breakdown process for each isomer. The percentages listed are the percent of the reactant that is consumed to produce the product shown, by all the reactions that can produce that product from the reactant, except where one particular reaction is noted. These numbers are determined by integrating the rate of production or consumption of each species by each reaction up to the point of 20 % fuel consumption, and normalizing each reaction by the total produced or consumed of each species up to that point. The 20 % fuel consumption point is chosen because it is before small molecule chemistry takes over to drive the ignition, and it has been used previously [6, 12]. The rates of production are taken from a CONV simulation, with initial conditions of 750 K and 15 bar as well as 750 K and 30 bar. These conditions are representative of typical conditions after compression in the present RCM experiments. The plain text percentages

on top of the arrows are the 15 bar case and the bold numbers underneath are for the 30 bar case.

In the following discussion, carbon-centered radicals are labeled according to their distance from the hydroxyl moiety in the fuel molecule, as shown in Fig. 1. As expected at the relatively low temperature of this analysis, H-abstraction reactions dominate over unimolecular decomposition for all four isomers. It is also expected that *n*-, *s*-, and *i*-butanol react primarily to their respective α -hydroxybutyl radicals, since the α C-H bond has the lowest energy [12]. Due to its unique structure, *t*-butanol does not have an α -hydroxybutyl radical that can be formed by H-abstraction, so *t*-butanol is primarily consumed to form the β -hydroxybutyl radical, because the O-H bond energy is much higher than β C-H bond energies.

The unique structure of *t*-butanol continues to affect the second level of reactions. In the temperature and pressure regime investigated, *t*-butanol tends to add to molecular oxygen at the carbon radical site, forming a hydroxybutylperoxy (RO_2) species. That this pathway is dominant is due to the fact that *t*-butanol has no α -hydroxybutyl radical. For the other three butanol isomers that do have an α -hydroxybutyl radical, the second level of reactions primarily produces an aldehyde + HO_2 by direct reaction—no hydroxybutylperoxy adduct is formed in this reaction, and there is no possibility for typical hydrocarbon low-temperature chain branching. Therefore, it is hypothesized that the pre-ignition heat release seen in *t*-butanol is caused by the oxygen addition to the fuel radical to form β -hydroxybutylperoxy, which is an exothermic reaction.

Figure 23 shows the total cumulative heat release of each isomer and the cumulative heat release of an important reaction for each of the isomers (inset), from a CONV simulation with initial conditions of 750 K and 30 bar; analysis of 15 bar results is substantially similar. The cumulative heat release in the inset is found by integrating the heat release by each reaction with respect to time, while the reactions shown are the respective reactions that have released the most heat up to the 20 % fuel consumption point for each isomer. The abscissa of the plot is the fuel conversion, in percent. This choice of x-axis allows a fair comparison of the heat release, because the ignition delays of each isomer are markedly different, so comparing the heat release with a time axis is more difficult. In Fig. 23, exothermicity is represented by positive quantities.

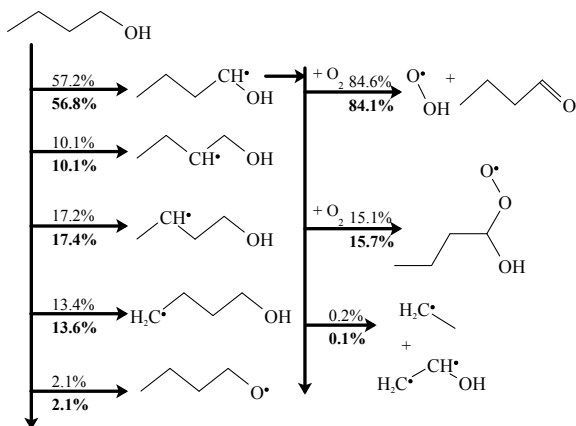


Figure 19: Pathway analysis for simulations of *n*-butanol at temperature of 750 K, in stoichiometric air, using the mechanism of Sarathy et al. [12]. Percentages in normal text represent an initial condition of 15 bar; bold text is for 30 bar.

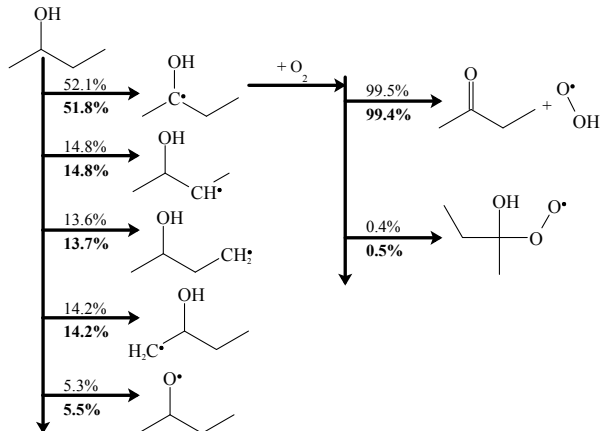


Figure 20: Pathway analysis for simulations of *s*-butanol at temperature of 750 K, in stoichiometric air, using the mechanism of Sarathy et al. [12]. Percentages in normal text represent an initial condition of 15 bar; bold text is for 30 bar.

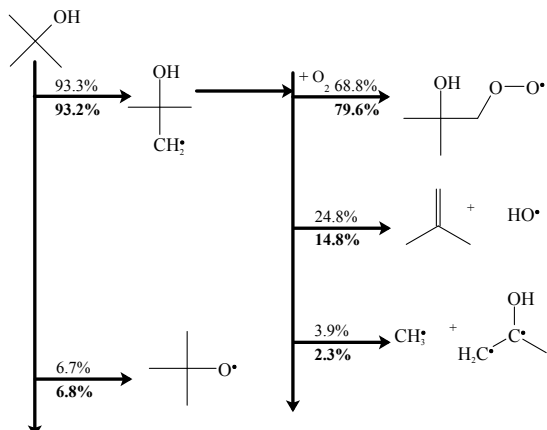


Figure 21: Pathway analysis for simulations of *t*-butanol at temperature of 750 K, in stoichiometric air, using the mechanism of Sarathy et al. [12]. Percentages in normal text represent an initial condition of 15 bar; bold text is for 30 bar.

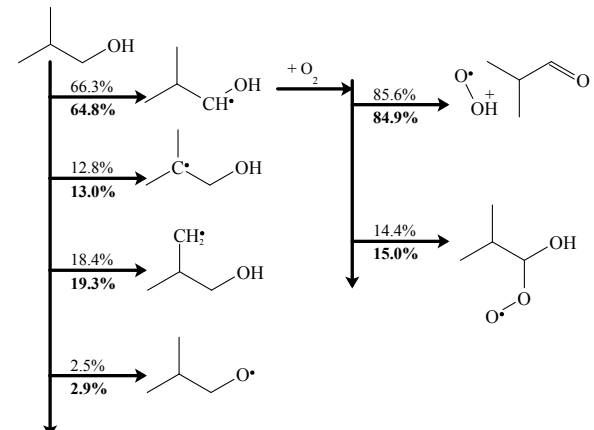


Figure 22: Pathway analysis for simulations of *i*-butanol at temperature of 750 K, in stoichiometric air, using the mechanism of Sarathy et al. [12]. Percentages in normal text represent an initial condition of 15 bar; bold text is for 30 bar.

Cumulative Heat Release, 750 K, 30 bar, $\phi = 1.0$

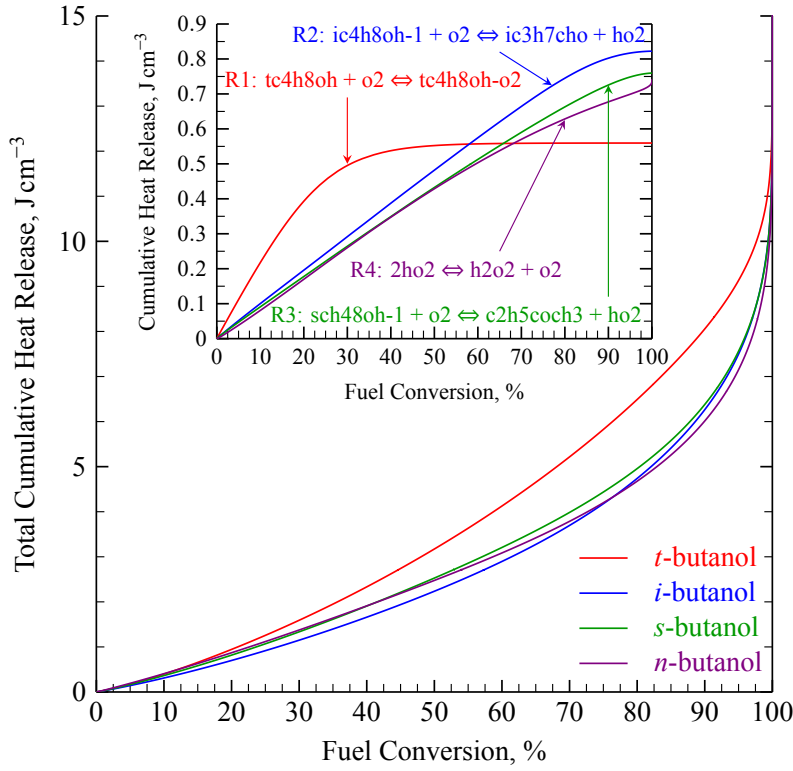


Figure 23: Total cumulative heat release and cumulative heat release by important reactions (inset) as a function of fuel consumption from a simulation using the mechanism of Sarathy et al. [12] with initial conditions of 750 K and 30 bar, in stoichiometric air. See Fig. 24 for definitions of reactions in the inset.

In Fig. 23, it is clear that *t*-butanol has higher heat release at low fuel consumption (during the induction period) than the other three isomers. In addition, the primary heat release reaction for *t*-butanol has created much more heat than the primary reactions of the other three isomers. As the reactions proceed, and the temperature increases, the reverse reaction in the *t*-butanol case becomes more important, and the heat release contribution of this oxygen-addition reaction levels off. The dominance of this reaction at early times is unique to *t*-butanol ignition, and appears to be driving the pre-ignition heat release.

Other researchers have also undertaken studies of the low to intermediate temperature combustion of *t*-butanol. Lefkowitz et al. [21] performed a study in the Variable Pressure Flow Reactor (VPFR) at Princeton University on the oxidation of *t*-butanol over the temperature range from 680 K to 950 K, at 12.5 atm and stoichiometric mixture conditions. It is interesting to note that they found no evidence

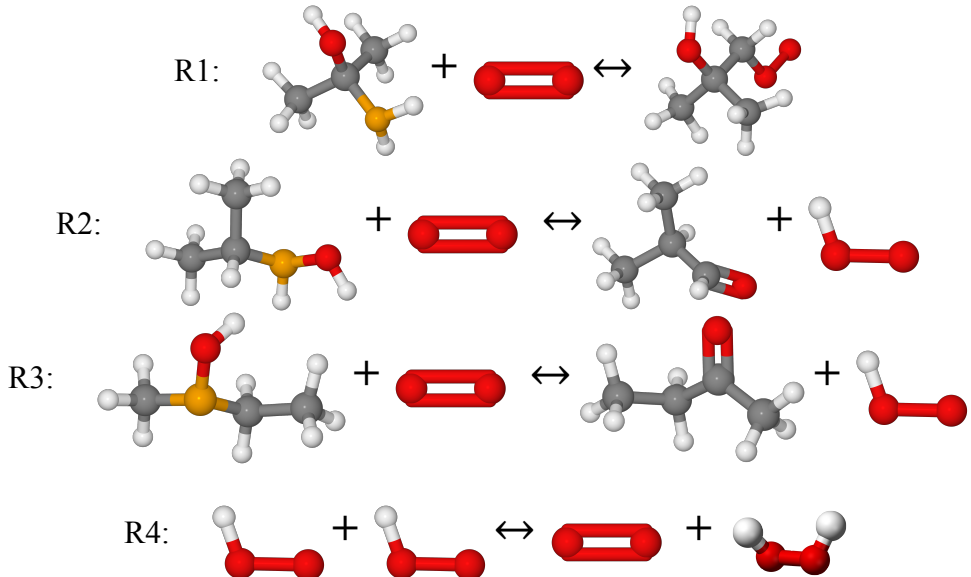


Figure 24: Reactions causing the most heat release in the ignition of the butanol isomers. The reaction number refers to Fig. 23.

of traditional hydrocarbon low temperature chemistry. They did, however, find significant quantities of acetone, peaking at approximately 800 K. Lefkowitz et al. [21] concluded that the primary pathways of acetone formation are tautomerization of propen-2-ol and β -scission of the alkoxy radical, based on an analysis of the mechanism from Grana et al. [16]. Both of these pathways are dependent on unimolecular decomposition of the hydroxybutyl radicals. However, this mechanism has only been validated for flame studies; indeed, an updated version of this model (by Frassoldati et al. [13]) is unable to predict the low-temperature ignition delays measured in this study and hence is not considered for analysis.

In contrast to the study of Lefkowitz et al. [21], path analysis of the mechanism by Sarathy et al. [12] shows that unimolecular decomposition of the hydroxybutyl radicals is not the most important pathway; as mentioned earlier, the most important pathway is the formation of β -hydroxybutylperoxy. Further analysis shows that the primary pathway of reaction of the *t*-butanol β -hydroxybutylperoxy species is through the Waddington mechanism. The Waddington mechanism has been shown experimentally to be an important pathway for β -hydroxypentylperoxy radicals in the low temperature combustion of *i*-pentanol [22], as well as the β -hydroxybutylperoxy radicals of *i*- and *t*-butanol [23]. *t*-Butanol only produces β -hydroxybutyl radicals, and one of the products of the Waddington

pathway in *t*-butanol is acetone (the others are formaldehyde and hydroxyl radical); over 88 % of the acetone produced up to the 20 % fuel consumption point is produced by the Waddington reaction. The study in the VPFR thus provides further evidence of the importance of low-temperature hydroxybutylperoxy chemistry in *t*-butanol, although it is not traditional hydrocarbon low-temperature chemistry.

Up to this point, the discussion has focused mainly on the importance of hydroxybutylperoxy chemistry in *t*-butanol. Nevertheless, the chemistry of the hydroxybutylperoxy species is important in the combustion of the other isomers of butanol as well. Using the high pressure ST at RWTH Aachen University, Vranckx et al. [24] showed the importance of peroxy chemistry pathways in the autoignition of *n*-butanol. By adding a lumped peroxy model to an existing kinetic model for *n*-butanol combustion, they were able to substantially improve agreement of the model with their experiments at high pressure and low temperature [24].

0.5.1 Comparison of *i*-Butanol Mechanisms

As discussed in Sec. 0.4.3, the Sarathy et al. mechanism [12] tends to under-predict the experimental ignition delays of *i*-butanol, whereas the MIT mechanism [20] tends to over-predict the experimental data. Some of the differences between the mechanisms are demonstrated by the path flux diagram shown in Fig. 25. The diagram is produced by the same procedure as Figs. 19–22, except the initial conditions of the simulation considered in Fig. 25 are 800 K and 30 bar for a stoichiometric mixture of *i*-butanol with air. The percentages in plain text are the results from a simulation with the MIT mechanism [20]; the percentages in italics are from a simulation with the Sarathy et al. mechanism [12].

Only the pathways for the α - and β -hydroxybutyl radicals are shown in Fig. 25; analysis of the γ -hydroxybutyl and isobutoxy radicals shows similar important pathways for both mechanisms. Figure 25 shows that there is a good agreement between the mechanisms in the first step of fuel decomposition, although the MIT mechanism tends to form slightly more β -hydroxybutyl and slightly less α -hydroxybutyl than the Sarathy et al. mechanism. The subsequent reactions of

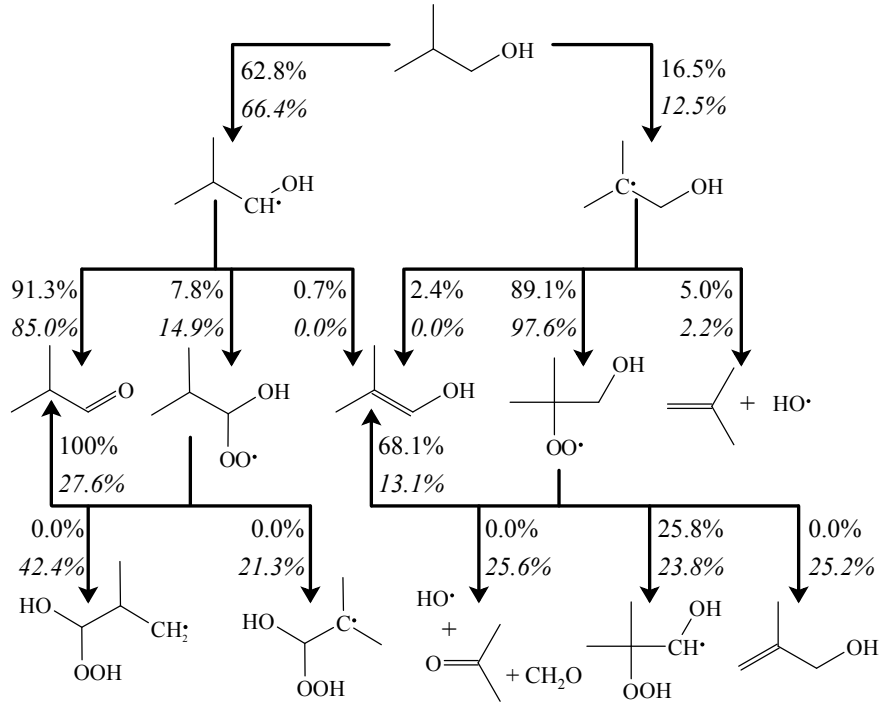


Figure 25: Path flux diagram for *i*-butanol/ O_2 /N₂, $\phi = 1.0$, 810 K, 30 bar. Plain text indicates the MIT mechanism [20]; italic text indicates the Sarathy et al. mechanism [12].

the primary fuel radicals are also similar between the mechanisms, although the formation of α -hydroxybutylperoxy occurs nearly twice as much in the Sarathy et al. mechanism as in the MIT mechanism.

In the third level of reactions, large differences between the mechanisms can be noted from Fig. 25. In the pathway of the β -hydroxybutyl radical, it can be seen that the breakdown of the β -hydroxybutylperoxy radical occurs partially via the Waddington mechanism to form acetone, formaldehyde and hydroxyl (OH) in the Sarathy et al. mechanism, whereas this pathway is not active in the MIT mechanism. This pathway is included in the MIT model but is not active under the conditions of this simulation.

Moreover, the fate of the α -hydroxybutylperoxy species is among the most important pathways in controlling the reactivity of the model and shows significant differences between the models. In the MIT mechanism, nearly all of the α -hydroxybutylperoxy goes to form isobutyraldehyde, which is itself the primary product of reactions of α -hydroxybutyl. This means that over 99 % of the α -hydroxybutyl radical is directed into the formation of isobutyraldehyde and hydroperoxyyl

(HO₂) in the MIT mechanism. However, in the Sarathy et al. mechanism, only about a quarter of the α -hydroxybutylperoxy goes to form isobutyraldehyde, and the rest is directed into traditional hydrocarbon low-temperature chain branching pathways leading to the formation of the hydroxyl radical.

The pathways involving α -hydroxybutyl and its products is of critical importance because the radical species produced from these pathways control the reactivity of the model. In the mechanism of Sarathy et al. [12], the radical that primarily controls *i*-butanol decomposition is hydroxyl, whereas in the MIT model [20], the reactivity is controlled by the hydroperoxyl radical.

In their work, Sarathy et al. [12] used the reaction rates computed by Silva et al. [25] for the hydroxyethyl system (i.e. ethanol as the parent fuel) to determine the rate of direct reaction of α -hydroxybutyl and oxygen to form aldehyde and HO₂, and then set the rate of oxygen addition to the α -hydroxybutyl radical (to form α -hydroxybutylperoxy) so that the total rate was less than the collisional limit. The rates of oxygen addition for the other radicals were prescribed depending on the type of carbon (primary, secondary, or tertiary) based on studies of butane and *i*-octane [12]. Based on the well-known importance of hydroxyl in driving the reactivity of combustion systems, and the sources of the estimates for the reaction rates of oxygen addition to hydroxybutyl (i.e. the entry to the pathway that controls the rate of hydroxyl formation), it can be hypothesized that the rates of hydroxybutylperoxy formation are overestimated in the mechanism of Sarathy et al. [12], as the simulated results under-predict the experimental data of *i*-butanol.

This hypothesis is supported by the results shown in Fig. 26, which shows the linear brute force sensitivity of the ignition delay (τ) of *i*-butanol with respect to changes in the A-factor of the rate coefficient, using the mechanism from Sarathy et al. [12]. The percent sensitivity is defined as the difference between the ignition delay when the A-factor of each reaction is halved and the nominal ignition delay, normalized by the nominal ignition delay, as shown below:

$$S_i = \frac{\tau(0.5A_i) - \tau(A_i)}{\tau(A_i)} \times 100\% \quad (1)$$

Therefore, negative sensitivity means that halving the A-factor of a reaction decreases the ignition

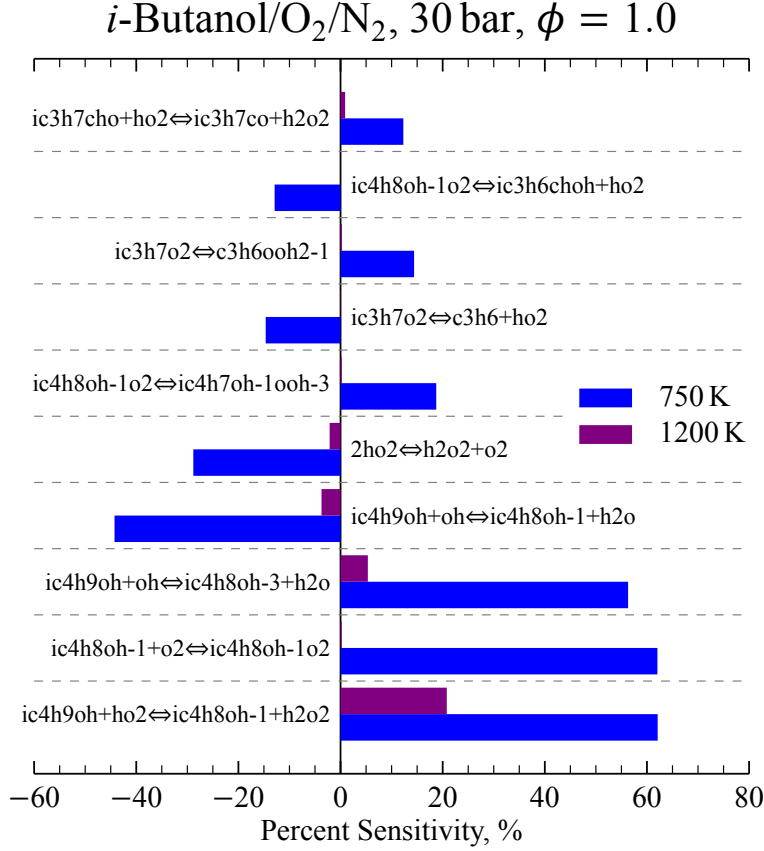


Figure 26: Linear brute force sensitivity analysis of the ignition delay with respect to the A-factors of the listed reactions in the mechanism from Sarathy et al. [12]. Positive quantities indicate the ignition delay is increased when the A-factor is halved.

delay, and positive sensitivity indicates the ignition delay increases. These results are for CONV simulations with initial conditions of 750 K and 30 bar as well as 1200 K and 30 bar.

The most sensitive reaction at the lower temperature is the initiation reaction of the fuel with hydroperoxyl radical to form the primary fuel radical and the second most sensitive reaction is the addition of oxygen to the primary radical. Both of these reactions have positive sensitivities, indicating that reducing the rate of these reactions increases the ignition delay and improves the agreement of the simulations relative to the experiments in this case. It is apparent, then, that reducing the amount of fuel propagating into the low temperature chain branching pathway of oxygen addition to the primary α -radical improves the simulated results. Interestingly, the *i*-butanol system is not sensitive to the rates of oxygen addition to the hydroxybutyl radicals other than the α -radical. At the higher temperature of 1200 K, there is little sensitivity on the ignition delay by

changing the rate of the oxygen-addition reaction, demonstrating its lack of influence at higher temperatures.

As a final comparison, we have modified this pathway in the mechanism from Sarathy et al. [12] so that the rate of oxygen addition to the primary fuel radical is arbitrarily set to zero; that is, the rate of the reaction $\text{ic4h8oh-1} + \text{o}_2 = \text{ic4h8oh-1o}_2$ is set to zero by zeroing the A-factor, while the rates of the other oxygen addition reactions were unchanged. This unphysical situation substantially changes the results of simulations for *i*-butanol—removing this pathway in the mechanism from Sarathy et al. [12] brings the simulations into close agreement with the ignition delay results from the MIT mechanism. In the MIT mechanism, the reactions of α -hydroxybutylperoxy exclusively produce *i*-butyraldehyde, whereas in the Sarathy et al. mechanism, some of the α -hydroxybutylperoxy radicals enter chain-branching pathways. Since the other oxygen addition reactions were unchanged, it is apparent that the addition of oxygen to α -hydroxybutyl is one of the controlling reactions for the high-pressure, low-temperature ignition of *i*-butanol using the mechanism of Sarathy et al. [12]. It is therefore concluded that a detailed examination of the rates of direct formation of aldehyde+HO₂ and oxygen addition to the α -hydroxybutyl radical are required to better predict the low-temperature ignition behavior of *i*-butanol. Furthermore, based on the other results of this study, a detailed analysis of the oxygen addition reactions to all the isomers of butanol is probably warranted.

0.6 Conclusions

In this work, ignition delays for all four isomers of butanol in stoichiometric mixture with air have been presented over the low to intermediate temperature range, and at two compressed pressures of 15 bar and 30 bar. The order of reactivity of the isomers is *n*-butanol>*s*-butanol≈*i*-butanol>*t*-butanol at the lower pressure, but changes to *n*-butanol>*t*-butanol>*s*-butanol>*i*-butanol at the higher pressure. This unexpected result is partially explained by the fact that there is substantial pre-ignition heat release present for *t*-butanol. To help understand the nature of the pre-ignition heat release of *t*-butanol, studies at off-stoichiometric conditions, $\phi = 0.5$ and $\phi = 2.0$ in air, are also conducted.

Comparisons of the experimentally measured ignition delays with two kinetic mechanisms show good agreement for certain isomers, but relatively poorer agreement for others. The kinetic mechanism of Sarathy et al. [12] is used to further elucidate the chemical processes controlling the autoignition of these butanol isomers. Pathway analysis of the fuel decomposition shows that *n*-, *s*-, and *i*-butanol primarily form α -hydroxybutyl radicals, because the proximity of the α carbon to the hydroxyl group reduces the C-H bond energy. The α -hydroxybutyl radicals tend to form an aldehyde plus HO₂ directly, without forming a hydroxybutylperoxy complex. However, due to its unique structure, *t*-butanol can only form β -radicals; these radicals do not have the tendency to react with oxygen to directly form HO₂ and an aldehyde. Rather, *t*-butanol preferentially adds oxygen to the fuel radical site. It is hypothesized that this reaction, O₂ addition to form hydroxybutylperoxy, causes the pre-ignition heat release in *t*-butanol and leads to a chain propagation pathway through the Waddington mechanism. The fact that this oxygen-addition reaction is preferred is unique to *t*-butanol, although a detailed understanding of the peroxy chemistry of alcohols is still of vital importance to the other butanol isomers. This is further demonstrated in this work for the case of *i*-butanol, where the ignition delay is quite sensitive to both the rate of primary fuel radical formation and to the rate of oxygen addition to the primary fuel radical. It is also noted that *n*-butanol autoignition was quite sensitive to peroxy chemistry in the study of Vranckx et al. [24].

All together, these analyses show the importance of the peroxy chemistry pathways in the autoignition of the butanols. Further experimental studies, such as species profiles from the low temperature ignition of the butanol isomers, could help reduce uncertainty in the pathways of fuel breakdown. Finally, further understanding of the rates of the peroxy pathways is important and therefore further theoretical and quantum chemical studies are warranted.